Title:
Characterization and Optimization of an Electro-thermal Microactuator for Precise Track Positioning

Authors:
Yang Fang, fanyang.nick@gmail.com, CGG Americas Inc.
Qikai Xie, qikai.xie@wsu.edu, Washington State University Vancouver
Xiaolong Zhang, xiaolong.zhang@wsu.edu, Washington State University Vancouver
Xiaolin Chen, chenx@wsu.edu, Washington State University Vancouver

Keywords:
Precise Positioning, Micromirror, Electro-thermal Actuation, Coupled Finite Element Model, Schematic System Behavior Model, Response Surface Optimization

DOI: 10.14733/cadconfP.2016.306-310

Introduction:
Micro-electro-mechanical systems (MEMS)-based mirrors are widely used in applications including optical displays, biomedical imaging, optical interconnects, optical switching, and laser beam steering [2, 4]. Compared to other driving mechanisms for MEMS mirrors such as electrostatic, electromagnetic and piezoelectric actuation, electro-thermal actuation has the major advantages of large displacement, large force, low actuating voltage, and low power consumption [3, 5]. Besides, their device fabrication process is relatively simple and fully compatible with the general integrated circuit (IC) fabrication process.

In this paper, we present a MEMS mirror actuated by four suspended electro-thermal bimorphs for optical data tracking of high-density storage application. Static, transient and dynamic characteristics of the microactuator are examined using coupled electro-thermal-mechanical finite element modeling as well as schematic system behavior modeling. The microactuator design is optimized using response surface methodology to achieve large actuation displacement, small lateral shift and adequate frequency response. Overall, the optimized design is shown to have an excellent linear relation between the micromirror deflection and input electric power, and can potentially be used as a fine-tracking device for high-density data storage applications.

Design and Fabrication Process Modeling:
We create the microactuator design using CoventorWare by taking the device manufacturability into consideration. A 3-D design geometry is developed by the deposition and etching of different layers of materials based on parameterized layout designs and standard photolithography steps. Fig. 1(a) shows the design layout, in which a $200\mu m \times 200\mu m$ micromirror is deposited on top of a $250\mu m \times 250\mu m$ substrate platform at the center and connected to four folded beams through two L-shaped metal heaters. Each folded beam has two identical arms. Each arm consists of a $125\mu m$ long silicon-dioxide-on-silicon bimorph section and a $115\mu m$ long aluminum-on-silicon bimorph section. Fig. 1(b) illustrates the critical process modeling steps. As shown in Fig. 1(b), a $2\mu m$ thick thermal oxide layer is deposited on the silicon wafer substrate as the sacrificial layer. The entire device is then covered by a $2\mu m$ thick doping silicon layer and then a $1.5\mu m$ thick silicon dioxide layer. Next, silicon dioxide and aluminum are patterned through photolithography to create the top layer of bimorph sections, respectively. Back side etching of silicon substrate is then performed, and the doping silicon layer of the bimorph beams is constructed by etching through the thermal oxide layer from the top side. Then, a thin film of gold is

sputtered on the device surface to form the micromirror and heaters. The final step is to strip off the sacrificial layer to release the suspension structure.

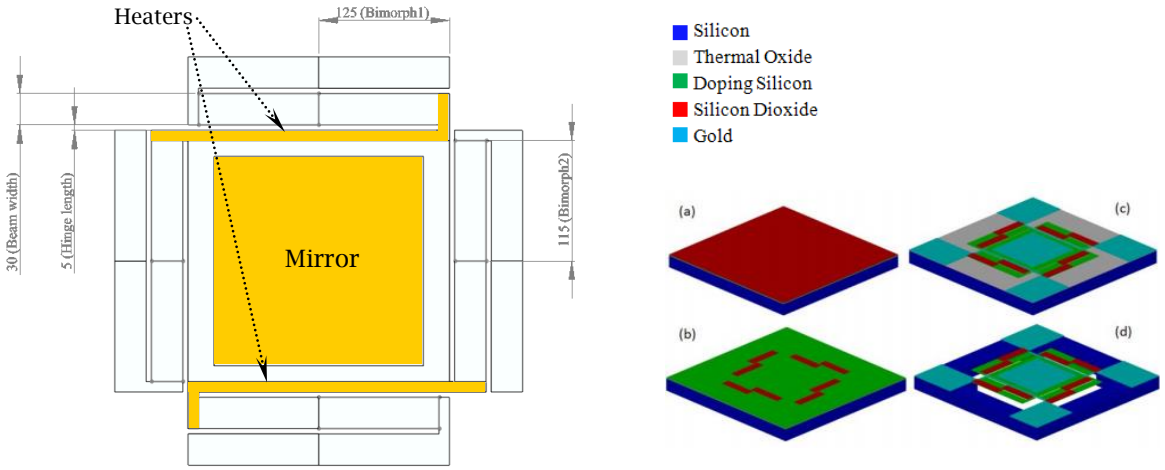

Fig. 1: Fabrication process based design modeling with figures from left to right: (a) 2D layout of the folded-beam microactuator (Unit: μm), (b) Deposition and etching of different material layers.

Coupled Electro-Thermal-Mechanical Analysis:

The developed microactuator model is analyzed to investigate its thermal and mechanical behaviors. Coupled electro-thermal-mechanical simulations are performed to determine the voltage, current density, temperature and deformation distributions of the micromirror actuator under a small voltage input, with resulted presented in Fig. 2. The boundary and initial conditions are given as follows: the folded beams are fixed at the four protruding ends, and the four fixed ends are assumed to be at a $20^{\circ}C$ room temperature. A $3V$ pulse voltage input with a $2ms$ pulse period composed of a $500\mu s$ on time and a $1500\mu s$ off time, is applied to two opposite ends of the folded beams, with the other two ends left grounded. The initial temperature of the whole structure is set up as the room temperature of $20^{\circ}C$. Based on the simulation, the mirror platform is found to be lifted up $1.6\mu m$ by the folded-beams under a $3V$ voltage input.

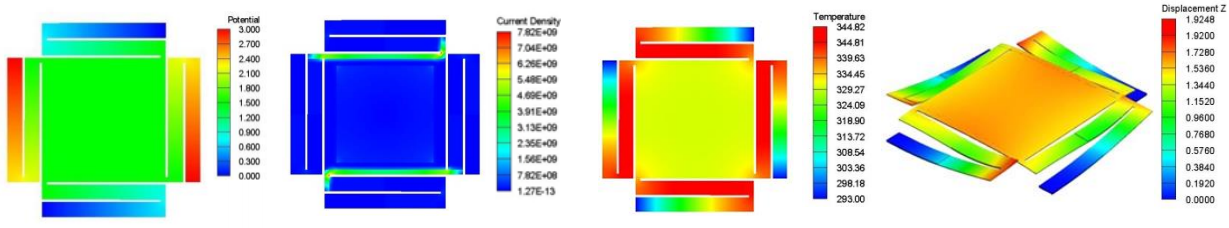

Fig. 2: Coupled finite element simulation results with figures from left to right: (a) Voltage distribution (unit: V), (b) Current density distribution (unit: pA/ μm^2), (c) Temperature distribution (unit: K), (d) Z-displacement distribution (unit: μm).

Response Surface Optimization:

Response surface optimization is performed for design trade-off evaluation. Two primary performance criteria of interest in the study are the mirror deflection and the mirror lateral shift. Maintaining mirror flatness is also important. However, this is ensured by the identical arm design in the folded

beam so that the deflected mirror is always flat as the suspension beam provides a zero rotation angle at the lifted end B (see Fig. 3).

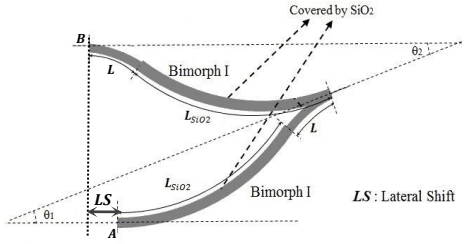

Fig. 3: The folded beam configuration.

The following two independent variables are chosen as design parameters: the length (*L*) of the aluminum-on-silicon bimorph section and thickness (*T*) of the aluminum layer. The design space is sampled through the central composite design (CCD), with the response dataset obtained for each design scenario through the coupled finite element simulation. The study levels of the CCD and corresponding values of design parameters are listed in Tab. 1. The same boundary conditions are applied to the coupled electoral-thermal-mechanical analyses as explained in the previous section. Tab. 2 gives the performance responses of the mirror deflection and the lateral shift for each combination of the design parameter levels.

Level	**-1.414**	**-1**	**0**	**1**	**1.414**
L (*μm*)	21.72	30	50	70	78.28
T (*μm*)	0.08	0.10	0.15	0.20	0.22

Tab. 1: Design parameter values of different levels for the optimization study.

No.	**L**	**T**	**Deflection (*μm*)**	**Lateral Shift (*μm*)**
1	-1	-1	2.5536	-0.0015
2	1	-1	5.4213	0.0244
3	-1	1	4.2691	0.0081
4	1	1	8.7138	0.1012
5	-1.414	0	2.5140	-0.0012
6	1.414	0	7.7413	0.0774
7	0	-1.414	3.5370	0.0024
8	0	1.141	7.1867	0.0533
9	0	0	5.4891	0.0230

Tab. 2: Experimental design and simulation results of the performance responses.

A quadratic response surface model in the form given in Eqn. (1) is used so that all the square terms and cross-product terms can be modeled [1].

$$Y = b_0 + \sum_i b_i x_i + \sum_i b_{ii} x_i^2 + \sum_{i<j} b_{ij} x_i x_j + \varepsilon \quad (1)$$

where Y stands for the performance response; $\mathbf{x_i}$ is the i^{th} controlled variable (design parameter), $\mathbf{b_i}$, $\mathbf{b_{ij}}$ are the i^{th} and ij^{th} estimated regression coefficient, respectively. ε is the error.

By applying least squares method, the response surface models for the mirror deflection (D) and mirror lateral shift (LS) can be obtained as follows:

$$D = 5.4891 + 1.8383L + 1.2713T - 0.1821L^2 - 0.0650T^2 + 0.3943LT \quad (2)$$

$$LS = 0.0230 + 0.0288L + 0.0198T + 0.0076L^2 + 0.0025T^2 + 0.0168LT \quad (3)$$

The design objective is set as to maximize the mirror deflection (D) under a lateral shift of no greater than 1% of the mirror deflection, i.e., $LS \leq 0.01D$. The optimal parameter settings are determined by applying sequential quadratic programming (SQP) optimization algorithm. Fig. 4 shows the infeasible and feasible design regions. The line with hash marks represents where *LS* equals to 1% of *D*. The optimal point is found to be at the location with coordinates of (0.5016, 1.3700), which correspond to $L = 60.03\mu m$ and $T = 0.22\mu m$. The optimal mirror deflection and the lateral shift can thus be found by Eqns. (2) and (3) as $8.25\mu m$ and $0.0825\mu m$, respectively.

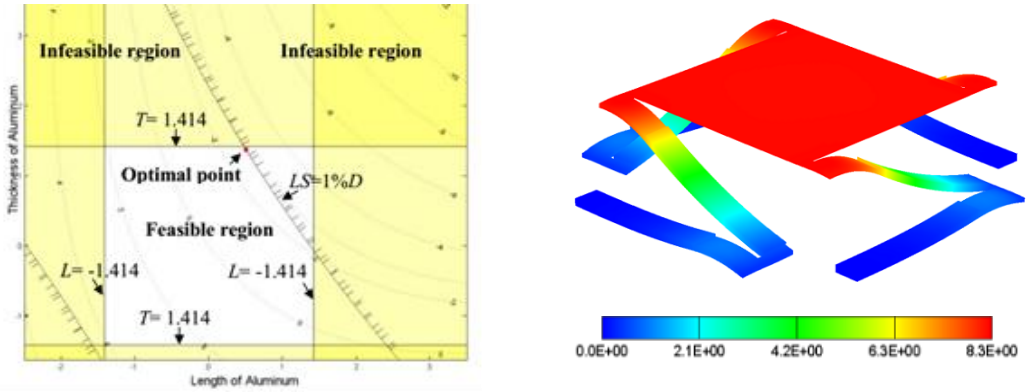

Fig. 4: Response surface optimization results with figures from left to right: (a) Design space, (b) Deformation plot of the optimum design.

An excellent linear relation of the electro-thermally induced mirror deflection and the input electric power is also observed from the design model investigation, as shown in Fig.5.

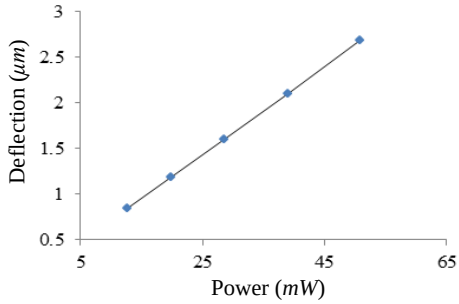

Fig. 5: Mirror deflection vs. input power.

Frequency Response Characterization:

For frequency-domain characterization of the electro-thermal microactuator, behavioral modeling is conducted to ensure that the device can support the servo bandwidth of a minimum of $10kHz$. Fig. 6(a) shows the schematic model developed for the microactuator. The frequency response presented in Fig. 6(b) shows that the fundamental resonant frequency of the optimized design is around $14.8kHz$, which meets the design criteria of having a high bandwidth of over $10kHz$ for servo control.

Conclusions:

In this work, design characterization and optimization are conducted on an electro-thermal bimorph-based microactuator. Coupled electro-thermal-mechanical simulation is carried out to investigate the effects of dimensional variations on device performance. Design of experiments and response surface optimization are utilized to determine the optimal parameter settings. The frequency domain behaviors are characterized by schematic system behavior models. Our results show that the optimized design is capable of generating a large mirror deflection of $8.25\mu m$, while maintaining

mirror flatness and introducing only a negligibly small lateral shift of 0.0825 μm. The resonant frequency of the optimized design is found to be 14.8kHz, which is adequate to support high servo bandwidth control. The microactuator also achieves an excellent linear relation between mirror deflection and input power. The design can be a good candidate, potentially used as an effective fine-tracking device for high-density data storage applications.

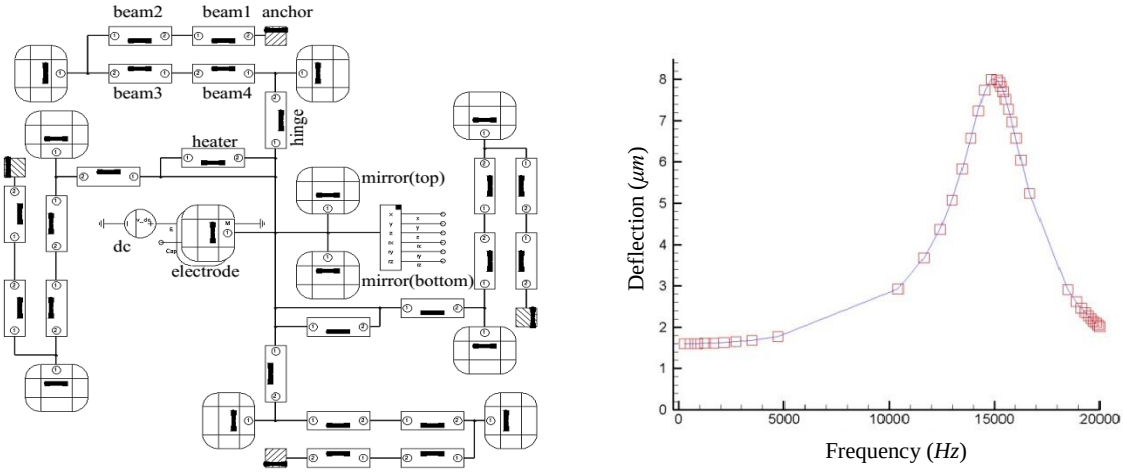

Fig. 6: System-level modeling with figures from left to right: (a) Behavioral model of the microactuator (b) Frequency response of the microactuator.

Acknowledgements:

We would like to express our sincere thanks to Dr. Jiaping Yang at A*STAR Data Storage Institute in Singapore for the helpful discussions he provided about the work.

References:

[1] Chen, S.; Yang, J.; Mou, J.;Lu, Y.: Quality based design approach for a single crystal silicon microactuator using DOE technique and response surface model, Microsystem technologies, 8(2-3), 2002, 182-187. doi 10.1007/S00542-001-0128-8

[2] Cheng, S.; Chou, P.: Adaptive ZPETC method for dual-stage actuator controller design in miniaturized optical disc drive, Proc. 2008 IEEE 14th International Mixed-Signals, Sensors, and Systems Test Workshop, 1-6. doi: 10.1109/IMS3TW.2008. 4581603

[3] Tsai, C.-H.; Tsai, C.-W.; Chang, H.-T.; Liu, S.-H.;Tsai, J.-C.: Electrothermally-Actuated Micromirrors with Bimorph Actuators—Bending-Type and Torsion-Type, Sensors, 15(6), 2015, 14745-14756. http://dx.doi.org/10.3390/s150614745

[4] Watanabe, I.; Ikai, Y.; Kawabe, T.; Kobayashi, H.; Ueda, S.;Ichihara, J.: Precise track-following control using a MEMS tracking mirror in high-density optical disk drives, Proc. 2002 International Symposium on Optical Memory and Optical Data Storage Topical Meeting, 2002, 257-259. http://dx.doi.org/10.1109/OMODS.2002.1028633

[5] Yang, J.; Deng, X.; Chong, T.: An electro-thermal bimorph-based microactuator for precise track-positioning of optical disk drives, Journal of Micromechanics and Microengineering, 15(5), 2005, 958-965. http://dx.doi.org/10.1088/0960-1317/15/5/009